IOSR Journal of Applied Physics (IOSR-JAP)
e-ISSN: 2278-4861.Volume 7, Issue 4 Ver. II (Jul. - Aug. 2015), PP 51-61
www.iosrjournals.org

The role of bismuth in the transport properties of amorphous $Ge_{20}Bi_xSe_{80-x}$thin films

Zeinab ELSayed ELMandouh[1], E.M. Abdelrazek[2],
Hesham Azmi ELMeleegi[1], Ahmed Hosny Hammad[1], Esaad Mohy ELdin[1.]
[1]*National Research Centre, Affiliation ID: 60014618, Phys. Dept .,El-Behoos. St.,Dokki,Cairo,(Egypt).*
[2]*University of Mansoura 35516 Phys. Dept.(Egypt).*

Abstract: *Amorphous $Ge_{20}Bi_xSe_{80-x}$thin films have been prepared on glass substrates by vacuum deposition. This system is promising candidate for application as a new generation of p-n junctions. Measurements of optical spectra; reflection and transmission during visible to near infrared region; as function of composition were done. The composition of the system was checked by EDAX. HR-Transmission electron microscope patterns, morphology and electron diffraction were introduced. The optical constants like the energy gaps were calculated and found to range from 0.36 e.V to 1.73 e.V. The energy gaps decreases via increasing thicknesses hence they fulfill the quantum size effect. The effect of Bi content on the energy gaps "Eg" is that it decreases with increasing Bi content. The dispersion energy Ed and the energy of the effective dispersion oscillator E_o were determined. Transport properties and thermoelectric power indicate the change of carrier type from p type to n type. DC conductivity for $Ge_{20}Bi_xSe_{80-x}$thin films was studied which shows that Bi affects drastically on σ_{DC} for the three compositions under investigation.*

Keywords: *HRTEM patterns, Optical Properties, Thermoelectric Properties, Electrical Conductivity, quantum size effect, Effect of Disorder Structure on Electrical Parameters.*

I. Introduction

Germanium chalcogenide glassy alloys belong to an interesting and unique class of amorphous materials and have wide applications in electronic and optoelectronic devices. The structural model describing GeSe glasses is based upon the Ge atoms of coordination four and selenium atoms of coordination two [1]. Amorphous chalcogenide glasses prepared by melt-quenching generally behave as p-type conduction as evidenced by thermo power measurements [2]. The addition of Bi or Pb[3,4] at certain atomic percentage into germanium based chalcogenide glasses causes the reversal of the conduction type. This has been attributed to the pining of the Fermi level towards the conduction band due to the upset of the equilibrium between negatively D^- and positively D^+ charged defect states [5]. The carrier type reversal (CRT) from p to n in semiconducting chalcogenide glasses is an important and along standing problem in glass science. Ge-Se glasses exhibit CTR when metallic elements Bi and Pb are added [6].

The photo induced changes in optical properties of Ge_{20} Se_{73} Bi_7 were studied. The refractive index has been analyzed according to Wemple- DiDominico single oscillator model and the value of E_o and E_d were determined. The photo structure effects were discussed in the light of single – double well model proposed by Tanaka and chemical bond approach[7] . Measurements of absorbance and transmittance in Ge_{20} Se_{80-x} Bi_x in the visible region were carried out. The optical energy gap decreases with increasing Bi- content is related to increase of Bi – Se bonds and the decrease of Se – Se bonds. The optical gap increases with increasing annealing time [8]. A study of the electrical and optical properties of amorphous Ge20 M_{75} Bi_5(M=S, Se or Te) has been investigated. A disturbance in the balance of C^- , and C^+ charged centers shifting the Fermi level from mid- gap is proposed. Incorporation of 5 at% Bi seems to have no drastic effect on the electronic structure as the Fermi level is still pinned at mid point[9].

Zehed , et al [10] measured electrical resistivity of $Ge_{20}Bi_x$ Se_{80-x} glasses where (x = 0 to 25). The electrical activation energy of the films was determined by investigating the temperature dependence of resistivity. A large decrease in the electric activation energy was observed as Bi content was increased up to 10 at %. The optical and electrical data explained that the addition of Bi produces localized states near the conduction band edge so the electrical transport is due to hopping of electrons after being excited into localized states at the conduction band edge. The linear refractive index and Wemple- DiDomenico parameters were used for the determination of non linear index in wavelength region of 400 to 1800 nm. The addition of Bi drastically increases non linear refractive index in Ge Se In three orders higher than silica glass [11]. The important aspect to be addressed in this context is the uniqueness of the role of Bi in Ge- Se glasses electrical, thermal and spectroscopic investigations onGe_{20} Bi_xSe_{80-x} glasses has been performed to arrive to the role of Bi.

II. Experimental

Bulk samples of $Ge_{20}Bi_xSe_{80-x}$(x = 5, 10, 15) were prepared by melt quenching technique. High purity (99.999%) elements with appropriate atomic percentage were sealed in silica ampoule in vacuum. The ampoule was kept in furnace for 24 hour at 1100 C^o. Thin films of various compositions of $Ge_{20}Bi_xSe_{80-x}$ were prepared by thermal evaporation technique. The amorphicity of the samples was confirmed by the absence of any sharp rings in the Electron-diffraction pattern taken by HRTEM. The thickness was measured by Scanning Electron Microscope, JXA-840A Electron Probe Micro- analyzer. The optical transmission and reflection spectra were recorded at room temperature for all samples using UV-visible double spectrophotometer, JASCO.Corp.V-570, in the range 300 to 2500 nm. The electrical measurements was done by Keithley 6517A electrometer, while, the thermoelectric phenomena was studied using special circuit to determine the thermoelectric efficiency.

III. Results

3.1 Morphology and structure:

TEM Pattern and selected area electron diffraction for as prepared $Ge_{20}Bi_xSe_{80-x}$ where; x = 5, 10, 15 which are shown in Plate [1(a, b, c)]. The whole matrix consists of particles with different shapes. The particles size was increased with increasing the Bi content; their contrast is uniform as expected for amorphous state. The amorphous nature was confirmed by the hallow rings observed in the electron diffraction.

3.2. Optical Properties:

Measurements of transmittance "T" and reflectance "R" of $Ge_{20}Bi_xSe_{80-x}$(where x = 5,10,15 at.%), thin films in the visible range at room temperature were carried out. Figure [1(a, b, c)] shows the transmission and reflection data of the three compositions which declare two absorption processes;

1. A high energy cut off due to inter-band transitions.
2. A low energy region which depends on the wavelengths due to free carriers absorption [12, 13, 14].

In order to determine the optical band gap, "Eg". The absorption spectra of the compositions were analyzed. The optical band gap can be driven from the spectral dependence of the absorption coefficient "α" [15].

Considering the validity of the equation:

$$(\alpha h\nu) = \beta(h\nu - Eg)^n \quad \text{.....(1)}$$

Where β is a substance parameter, h is Planck constant, and ν is the frequency. The value of the power factor , n, is governed by the mechanism of the electrons transitions. In amorphous chalcogenide direct transitions are observed at n=0.5 while n=2 for indirect allowed transitions. The absorption coefficient (α) in equation (1) was calculated from equation (2)[16].

$$T = (1-R)^2 \exp(-\alpha d) \quad \text{.....(2)}$$

Where T : is the transmittance, R: is the reflectance, α: is the absorption coefficient ,and d: is the film thickness. Figure [2 (a, b, c)] shows the values of the calculated absorption coefficient α as function of wavelength for different compositions of $Ge_{20}Bi_xSe_{80-x}$. These curves exhibit a distinct feature that is the values obtained for α are fairly high ($\alpha = 2 \times 10^4$ to 1.2×10^5) which is the case for most high carrier concentration semiconductors. Figure [3 (a, b, c)]: represents plots of $(\alpha h\nu)^{0.5}$ vs. hν for films of $Ge_{20}Bi_xSe_{80-x}$; where x = (5, 10, 15). The intersection of the straight line with high energy points hν, in the graph of $(\alpha h\nu)^{0.5}$ versus hν , with the energy axis ; gives the energy gaps that are included in Tables 1 and 2 and; 3 . It is revealed from the tables that the quantum size effect was achieved indicating that the values of Eg decrease with increasing thickness. Such a behavior agrees well with equation [17]:

$$\Delta Eg = \frac{h^2}{8m^* t^2} \quad \text{.....(3)}$$

Where t: is the film thickness and m* is the effective mass. Mott and Davis gave evidence [18] that in many amorphous materials n should equals 2 in formula (1) which is readily obtainable by relaxing the requirement of conservation momentum in the derivation of α which shows a great agreement with Dunstan [19]. High doping impurity concentration affects the shape of the band edges of a semiconductor. The distribution of valence and conduction band states can be considered "smeared out" at the band edges: "band tails" which effectively reduces the width of the band gap. A calculation of the band gap narrowing ΔEg as a function of doping concentration N has been given by the equation [20]:

$$\Delta E_g(N) = \frac{3e^2}{16\pi\varepsilon}\left[\frac{e^2 N}{\varepsilon KT}\right]^{1/2} = \frac{3e^2}{16\pi\varepsilon L_D} \quad \text{.....(4)}$$

Where: ε: is permittivity of semiconductor, L_D is the screening "Debye" wavelength. Figure [4 (a, b, c)] shows the variation of optical refractive indices n vs. wavelength for different compositions. The value of k was determined from:

$\alpha = 4\pi k/\lambda$.....(5)

Where k: is the extinction coefficient, α: is the absorption coefficient, and λ: is the wave length. The refractive index, n, has been calculated from [21]:

$$n = \left(\frac{1+R}{1-R}\right) + \sqrt{\frac{(1+R)^2}{(1-R)^2} - (1+k)^2} \quad \text{..... (6)}$$

From [4]; refractive index n show that; n decreases with increasing wavelength while it increases with increasing thickness and, tends to saturate at high values of the wavelength.. Wemple etal.[22]. Used a single oscillator description of the frequency dependent dielectric constant to define the dispersion energy parameters E_d and, E_o. The relation between refractive index n and the single oscillator strength below the band gap is given by:

$$\frac{1}{n^2 - 1} = \frac{E_o}{E_d} - \frac{h\nu^2}{E_o E_d} \quad \text{.....(7)}$$

Where: E_o is the energy of effective dispersion oscillator, E is the photon energy and, E_d is the dispersion energy which indicates the average strength of the inter-band optical transition. Figure [5] shows the relation between ($n^2 - 1$) and ($h\nu$)^2 for all compositions. The values of E_o and E_d are directly determined from the slope ($E_o\ E_d$)$^{-1}$, and the intercept was (E_o / E_d). The values of E_o and E_d were listed in table 1,2,3 for all compositions under investigation. From data in table 1; E_o and E_d decrease with increasing thickness for sample 1 while for sample 2 table 2; E_o and E_d increase via increasing thickness. For table 3 sample 3 values of E_o and E_d have a slight change via thickness. The value of refractive index when hv tends to zero "n_o" and the optical high frequency dielectric constant, ε_∞ (= n_o)^2 are listed in tables.

3.3. Thermoelectric properties:

Measurement of thermoelectric power as a function of temperature provides the most direct way to determine the temperature coefficient of activation energy of thermoelectricity which is indeed the Fermi-energy by which we determine the mechanism of conduction. Thermoelectric power of disordered chalcogenides has shown to be P-type conduction in most cases. The addition of bismuth changes the conduction to be N-type instead of P-type at certain concentration. This Bi enters the network as charged species; changing the ratio of valence alternation pairs to such extent that the Fermi energy level gets unpinned. When the concentration of charged additives exceeds that of the valence alternative pairs; disordered chalcogenides can exhibit the carrier-type reversal phenomenon (or ; P to N conduction type transition). To chose thermoelectric material with optimum thermoelectric - energy conversion efficiency; we studied the parameters consisting of this efficiency. The effect of compositions of thin films ; $Ge_{20}Bi_xSe_{80x}$; samples on Seebeck Coefficient vs. temperature could be expressed as in figure [6 (a, b, c)], and was calculated from the following equation:

$$S = \pm\frac{k}{e}\left[\frac{\Delta E_f}{KT} + A\right] \quad \text{.....(8)}$$

Where: (e is the electronic charge), (K: Boltzmann constant),(ΔE_f = The activation energy of thermoelectric power; which is also the Fermi energy), and; (A: is a constant depending on the scattering mechanism). Figure [6 – a] illustrates Seebeck coefficient for samples of $Ge_{20}Bi_5Se_{75}$ under investigation which shows positive sign conduction from room temperature up to 393'Kelvins; which indicates that hole conductivity is a dominant in this range of temperatures, while Figure [6 – b] represents thermoelectric power 'TEP' for $Ge_{20}Bi_{10}Se_{70}$ where the curve shows negative sign indicating electron conduction, and TEP increases by increasing temperature from room temperature up to 393'Kelvins this Bi concentration have the highest value for TEP. Increasing concentration of Bi to 15% by wt. didn't alter the electronic conduction type of the sample till 403'Kelvins as represented in Figure [6 – c] where TEP increases first and then decreases.

Slack [23] has described the chemical characteristics of materials that might be candidate for good thermoelectric material; such candidates need to be narrow band gap semiconductors with high mobility carriers and low thermal conductivity. The total thermal conductivity is given by:

$$\frac{K_{thermal}}{\sigma_{electrical}} = LT = \left(b + \frac{5}{2}\right)\frac{K_b^{\,2}}{e^2}T \quad \text{.....(9)}$$

where: $K_{thermal}$: is thermal conductivity, L: Lorentz factor ,K_b: is Boltzmann constant, σ: is the electrical conductivity and, b: scattering factor=1.5 for intrinsic semiconductors. Figure[7 (a, b, c)] illustrates the behavior of thermal conductivity with increasing temperature figure [7 – a] shows exponential trend of $K_{thermal}$ with temperature; indicating two mechanisms of conduction; extrinsic one with lower slope " lower activation energy" at low temperatures , and intrinsic one with higher temperatures and a higher slope due to energy gap. While; for sample $Ge_{20}Bi_{10}Se_{70}$ thermal conductivity decreases with temperature which proves degeneracy we calculate $\Phi = E_f / k_bT$ with temperature in the range which thermoelectric parameters had been measured and it is clearly lied in the degenerate semiconductors and semimetals range i.e.; less than four and greater than minus four as shown in Figure [7 – b]. In Figure [7 – c] thin films of $Ge_{20}Bi_{15}Se_{65}$has the largest thermal conductivity and it increases with increasing temperature. The parameter Z represents the figure of merit for thermoelectric materials which is defined as :

$$Z = S^2 * \sigma_{electrical} / K_{thermal} \text{.....(10)}$$

Figure [8 (a, b, c)] represents figure of merit "Z" of samples under investigation. Figure [8 – a] shows a hump for Z with increasing temperature till 331'Kelvins and then decreases. While for $Ge_{20}Bi_{10}Se_{70}$ Figure [8 – b] shows the highest figure of merit but it decreases with increasing temperature. For samples $Ge_{20}Bi_{15}Se_{65}$ it decreases with increasing temperature. To increase the efficiency; figure of merit should increase via increasing thermoelectric power "S" or electrical conductivity "$\sigma_{electrical}$ " ; or by reducing thermal conductivity "$K_{thermal}$". Figure [9 (a, b, c)] shows the relation between optimum efficiency "η" and temperature "T". Where [24]:

$$\eta = \frac{\Delta T}{T_h}\left(\frac{M-1}{M + T_o/T_h}\right) \quad \text{.....(11)}$$

$$M = \left[1 + Z\left(\frac{T_h + T_o}{2}\right)\right]^{1/2} \quad \text{.....(12)}$$

Where : T_h is the hot end temperature of specimen and, T_o the cold end temperature of it.
$\Delta T = T_h - T_o$, and, Z: is the Figure of Merit.

Figure [9 – b] reveals that optimum efficiency has its best values for concentration of Bi at x = 10% and it increases with temperature. Doping of chalcogenide glasses may be possible after understanding the very different defect chemistry in these materials. The majority of experimental result can be explained by supporting that some of the normally two fold coordinated chalcogen atoms are present as positively charged three fold coordinated and negatively charged one-fold doping coordinated atoms. The property of moving Fermi-energy level by controlling the doping revealed a lot of amorphous semiconductors properties.

3.4. D.C-conductivity at high temperatures:

Bismuth dopant affects strongly on the conductivity behavior of $Ge_{20}Bi_xSe_{80-x}$. Figure [10 (a, b, c)] shows the composition dependence of electrical conductivity on temperature. Figure [10 - a] shows the curve of $\sigma_{electrical}$ as a function of temperature for intrinsic semiconductor containing an active impurity. The region ab corresponds to room temperatures and extended to the temperature of impurity depletion T_s while region bc stretched from impurity depletion temperature to temperature of transition from extrinsic to intrinsic conduction type T_i in this "plateau like" region all impurity atoms are ionized. The angle of incline of the curve indicates the high doping. While the region cd corresponds to intrinsic conduction in which charged carriers are practically equals to the impurity dopant atoms concentration at high temperature region.

$$\sigma = \sigma_0 \exp\left(\frac{Eg}{K_b T}\right) \quad \text{……(13)}$$

In Figure [10 - b]: the conductivity of sample $Ge_{20}Bi_{10}Se_{70}$ shows thermal switching behavior from high conductivity values at low temperatures to low conductivity values at high temperatures then it tends to saturate. This sample; $Ge_{20}Bi_{10}Se_{70}$; is an example of a degenerate semiconductor since it is highly doped so that the individual impurity atoms may become close enough neighbors that the doping energy levels merge into an impurity band and the behavior of such system ceases to show the typical traits of a semiconductor. On the other hand; sample $Ge_{20}Bi_{15}Se_{65}$represents a semiconductor trend as the conductivity increases with increasing temperature. The discrepancy between the activation energies calculated from d.c.conductivity and those calculated from thermoelectric power has been considered to be caused by one of the following conduction mechanisms which are: non-bipolar conduction[25],thermally activated mobility of predominant carriers[26] ,hopping of small polarons[27,28],or conduction in long range potential fluctuations[29]. From table 4; we noticed that the Fermi energy is of the order of magnitude or lower than the activation energy and this means that the mechanism of conduction is by thermally activated mobility[24] or by small polaron hopping[26]. But from calculations of E and E_μ using the chalcogenide model we deduce that they are in the same order of magnitude and nearly equal so, this indicates that the main conduction mechanism is thermally activated mobility one[29,30].

Calculations for a-chalcogenides data in table 4:

$E=E_a-\Delta E_f$……(14)

Where: E is the effective potential barrier height resulting from perturbation of bands due to disordered structure and, high density of charged defects.

Since;

$$\sigma_0 = eN_0(E)\mu_0 \quad \text{……(15)}$$

And[30];

$$N_0(E) = N_0 \frac{4}{\sqrt{\pi}}\left(\frac{E}{kT}\right)^{1/2} \quad \text{……(16)}$$

Where [30] ;

$$N_0 = 2\left(\frac{2\pi m_0 kT}{h^2}\right)^{3/2} \quad \text{……(17)}$$

Hence; total mobility could be calculated from:

$$\mu_T = \mu_0 \exp\left(\frac{-E_\mu}{kT}\right) \quad \text{……(18)}$$

Where [31];

$$Ln(\sigma_{electrical}) + \frac{eS}{k} = Ln(\sigma_0) + A - \frac{E_\mu}{kT} \quad \text{……(19)}$$

All parameters above were mentioned previously.

IV. Conclusion

Structural, Optical properties, Electrical and Thermo electrical Properties were investigated for Thin Film alloys of the chalcogenides: Ge20 Bix Se80-x for three concentrations of Bi included; x = 5,10,15; all of them have amorphous structure. Bismuth concentration affects greatly on energy gap values and quantum size effect were achieved for the three compositions as a result of thin film nature where Eg decreases with film thickness. The samples with x>=10 shows degenerate nature due to high dopping effect. The mechanisms of conduction was thermally activated hopping. Bismuth doping changes the conduction type from p-type at x = 5 to n-type for x = 10 and 15. Thermoelectric energy conversion efficiency and thermoelectric power values with temperature reveals that the composition x=15 is the best for application.

References

[1]. Trone, P.; Bensoussan, M. ; Brenace, A. Phys. Rev. B**, 1973**, 8,5947.
[2]. Frumar, M.; Tichy, L. J. noncryst. Solids, **1987**, 97/98, 1139.
[3]. Tonge, N.; Minami, T.; Tanaka, M. J. Noncryst. Solids **1980,**37, 23.
[4]. Tohge, N.; Matsuo, H.; Tanaka, M. J. Noncryst. Solids **1985**,96, 809.
[5]. Tohge, N.; Minami,T.; Tanaka, M. J. Noncryst. Solids **1980**,38/39 283.

[6]. Tohge, N.; Minami, T.; Tanaka, M. J. Noncryst. Solids, **1980,**38/39 () 238.
[7]. Ticky L.; Ticha, H. Solid State Commun. **1985** ,53, 238.
[8]. Al-shazly, O.; Hafiz, M.M. Journal of Material Science-Materials in Electronics **2001**,12, 7,395-401.
[9]. Seddik, K.; Fadel,M. Thin solid film**, 1993**,229,2,p223-226.
[10]. Sharma, I.; Tripthi, S.K.; Barman, P.B; Smith, R.A. Journal of Appl.Phys., **2011,**10,4,043108.
[11]. El.Zahed, H.; EL Korashy, A. Thin Solid Films, **2000** ,376,236.
[12]. Moss, T.S. Optical properties of Semiconductors, Butter Worth, London1959.
[13]. Moss, T.S.; Burell,G.J.; Ellis,B. Semiconductor Optoelectronics, Butter Worth, London1973 ,.
[14]. Smith, R.A. Semiconductors, Cambridge United Press London Chapt.7,1968.
[15]. Keireev, P.S. Semiconductor Physics, Mir Publishers- Mosco1974.
[16]. Becker,M.; Fan,H.Y.; Phys. Rev. **1949** ,76,1530.
[17]. Bhatt,V.P.; Giresesan, K.; Desai, C.F. Cryst.Res.Technol. **1989** ,24,2,187-192.
[18]. Mott, N.F.; Davis, AE.A.;Street, R.A. Phil.Mag. **1975** ,32,961.
[19]. Dunstan, D.J. J.Phys. **1983** ,c16; L567.
[20]. Tauc, J. In Amorphous and Liquid Semiconductors p.159, J.Tauc- Plenum Press. N.Y,1974.
[21]. Singh D.; Kumar J.;and, Thangaraj R. J.Non-Cryst. Solids, **2012** ,358, 2826-2834.
[22]. Wemple, H.S.; Didomenico, M. J.Physics.Review, **1971** ,B,3, 1338.
[23]. Slack, G.A."New Materials and Performance Limits for Thermoelectric Cooling – RoweDM(ed) CRC Handbook of Thermoelectrics ", CRC Press, Boca Raton FL, p.407-40.
[24]. Jain, G.C ; Berry, W.B. Transport Properties of Solids and Solid State Energy Conversion, Tata-Mc.Grow-Hill Publishing Co. LTD., Bombey-NewDelhi (1972).
[25]. Tohge, N.; Minami, T.; Tanaka, M. Japanese J. of Appl Phys, **1977**,16,977.
[26]. Amin,D.; Seager, C.H.; Quinn, R.K. Phys. Rev.Lett, **1972** ,28,813 .
[27]. Mahadevan, S.; Rao,K.J. J.Non-Cryst.Solids, **1972** ,34,53.
[28]. Overhof ,H. ; Beyer,W. Phylos.Mag. **1984** ,B49,L9.
[29]. Fritzsche, H. Amorphous and liquid semiconductors,edited by: J.Tauc, Plenum Press-New York1971.
[30]. Boer,K.W. Physica status solidi, **1969** ,34,721.
[31]. Weclewicz, Cz.; Zdanowicz, L. Thin Solid Films, **1987** ,151,87.

Figures and Captions:

Plate 1: HRTEM shots with diffraction pattern inside For Ge(20)Bi(x)Se(80-x)Thin Films.
Figure [1]: Transmission and reflection For Ge(20)Bi(x)Se(80-x)Thin Films
Figure[2]: Absorption coefficient vs. Wavelength for Ge20BixSe80-x
Figure[3]: Tauc behaviour against photon energy For Ge(20)Bi(x)Se(80-x)Thin Films
Figure[4]: Refractive index vs. wavelength for Ge20BixSe80-x Thin Films
Figure[5]: Reciprocal-squared refractive index-1 vs. photon energy for Ge20BixSe80-x Thin Films
Figure[6]: Thermoelectric power vs. Temperature of the hot end for Ge20BixSe80-x Thin Films
Figure [7]: Thermal conductivity vs. Temperature for Ge20BixSe80-x Thin Films
Figure[8]: Figure of Merit vs. Temperature for Ge20BixSe80-x Thin Films
Figure[9]: Thermoelectric energy conversion optimum efficiency vs. temperature for Ge20BixSe80-x Thin Films.
Figure [10]: Electrical conductivity vs temperature. for Ge20BixSe80-x Thin Films.

Plate[1]:

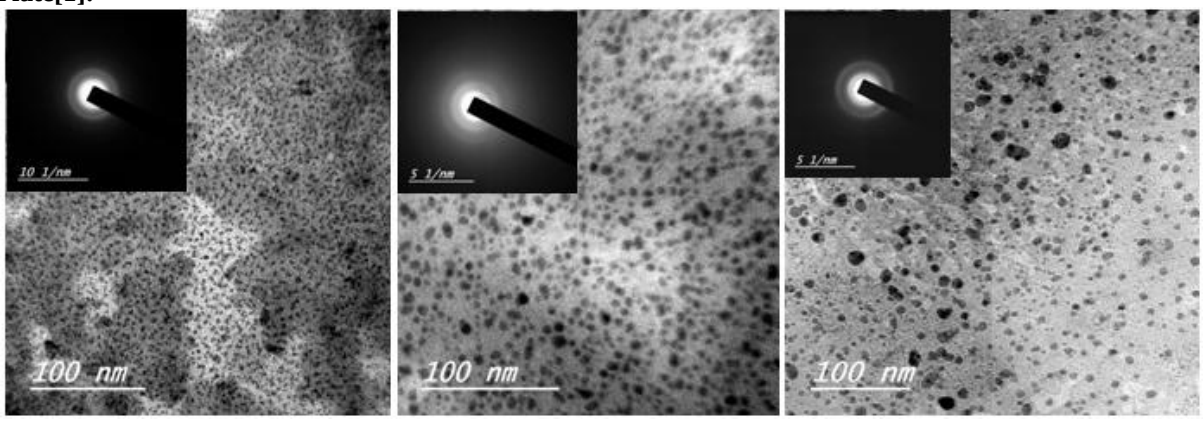

X = 5 **x = 10** **x = 15**

Plate 1: HRTEM Shots with diffraction pattern inside For Ge(20)Bi(x)Se(80-x)Thin Films.

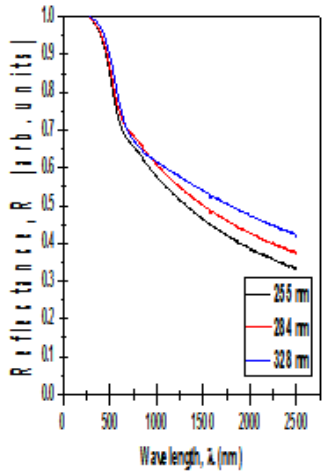

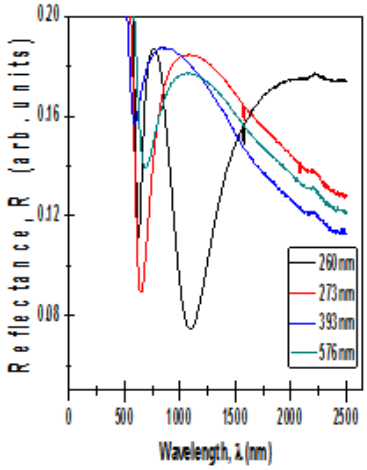

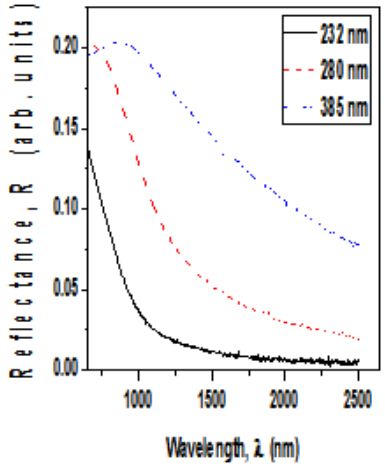

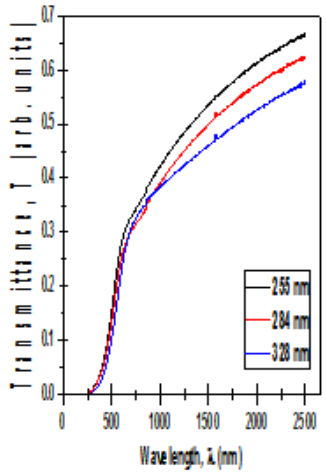

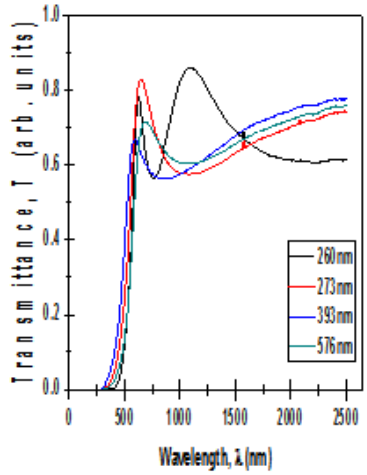

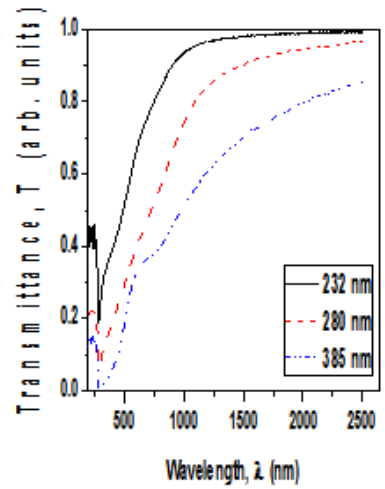

Figure [1-a]: Transmission and Reflection for Ge(20)Bi(5)Se(75).

Figure[1-b] Transmission and Reflection for Ge(20)Bi(10)Se(70)

Figure [1-c]: Transmission and Reflection for Ge(20)Bi(15)Se(65)

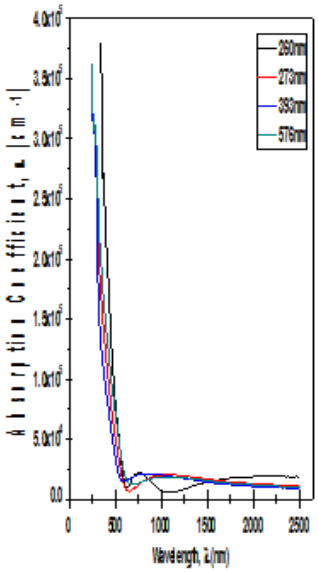

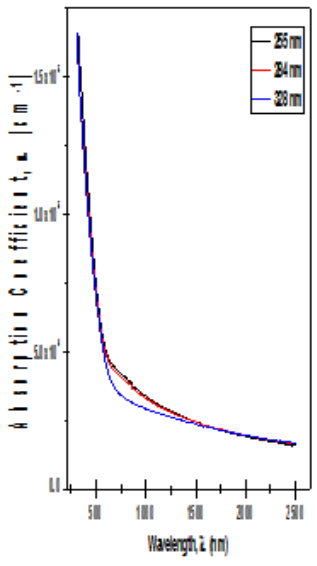

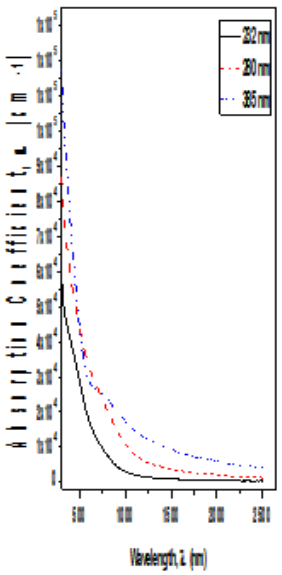

Figure[2-a] X = 5

Figure[2-b] X = 10

Figure[2-c] X = 15

Figure[2] Absorption Coefficient vs. Wavelength for $Ge_{20}Bi_xSe_{80-x}$ Thin Films

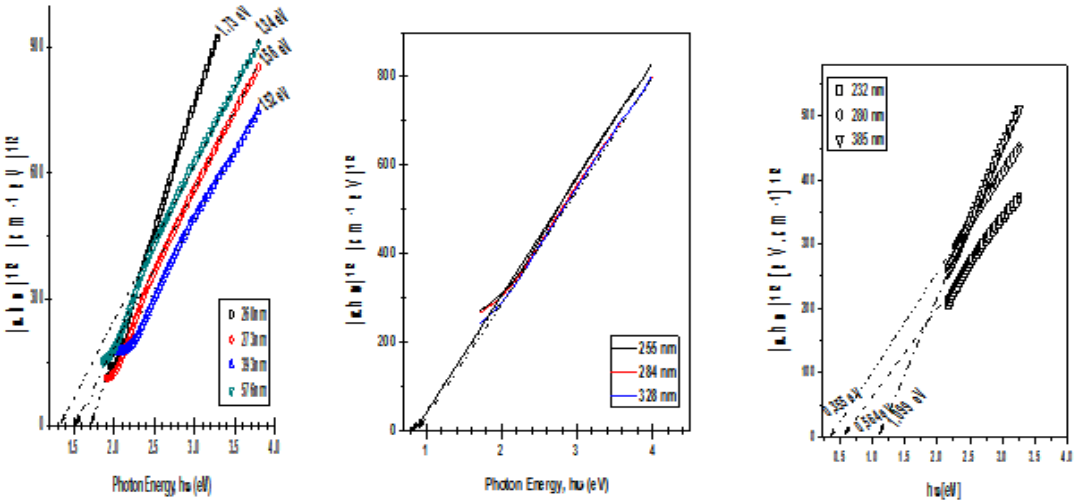

Figure[3-a] **Figure[3-b]** **Figure[3-c]**
X = 5 **X = 10** **X = 15**

Figure[3] Tauc behaviour against Photon Energy For Ge(20)Bi(x)Se(80-x)Thin Films

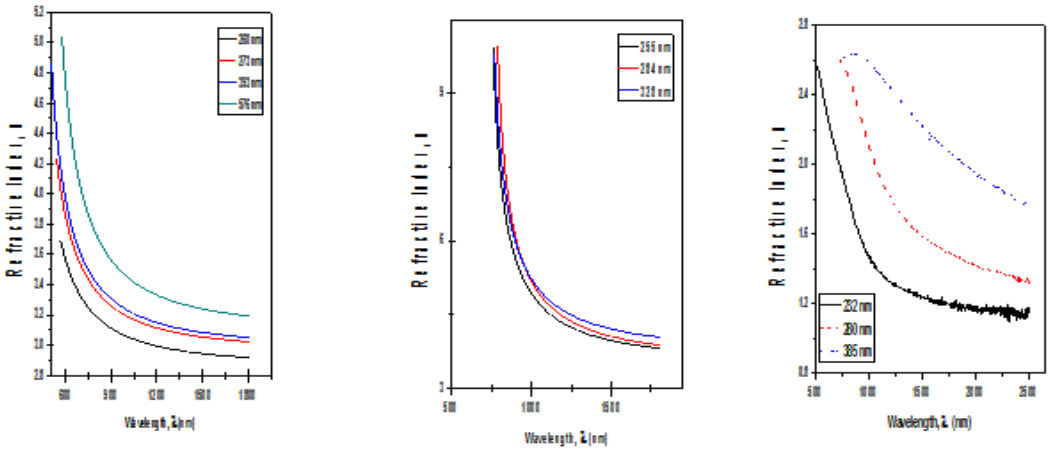

Figure[4a] **Figure[4-b]** **Figure[4-c]**
X = 5 **X = 10** **X = 15**

Figure[4] Refractive index vs. Wavelength for $Ge_{20}Bi_xSe_{80-x}$ Thin Films

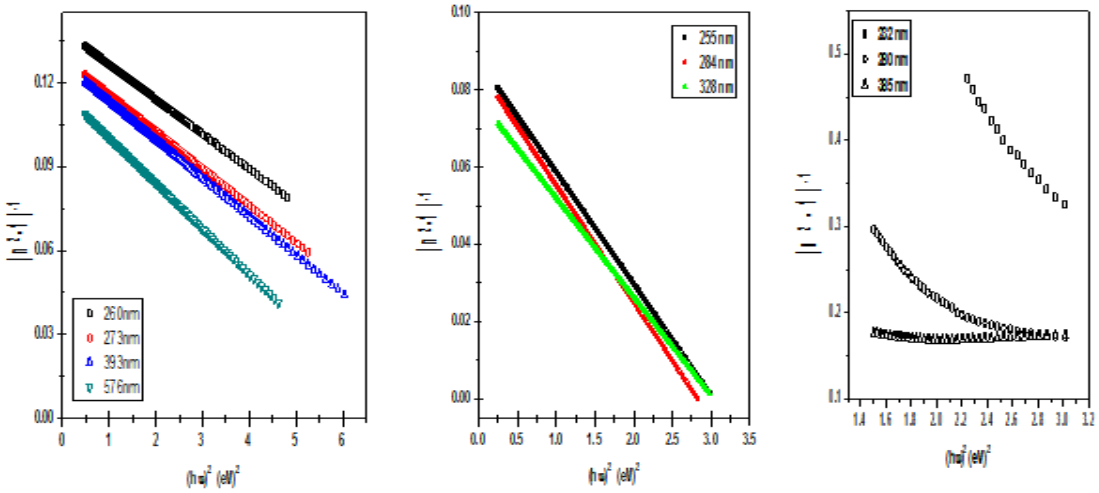

Figure[5-a] **Figure[5-b]** **Figure[5-c]**
X = 5 **X = 10** **X = 15**

Figure[5] Reciprocal-Squared Refractive index-1 vs. photon energy for $Ge_{20}Bi_xSe_{80-x}$ Thin Films

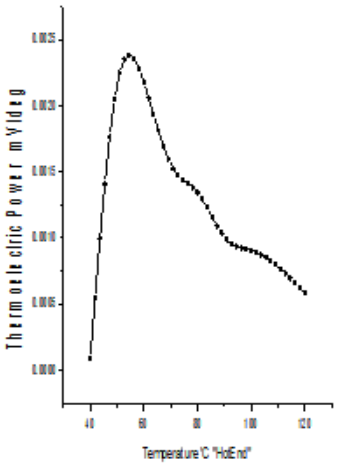

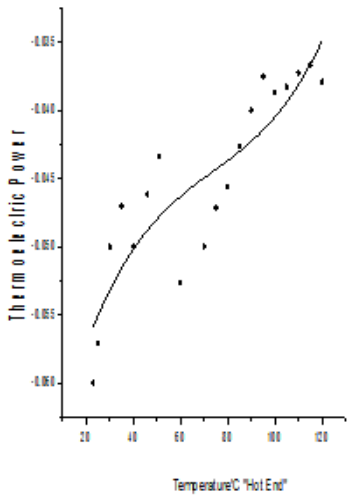

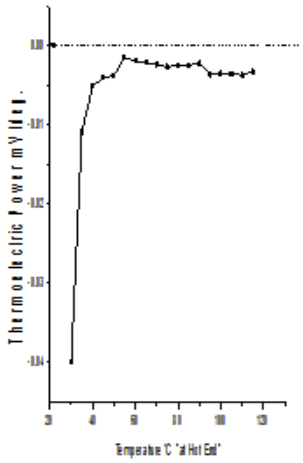

Figure[6-a] **Figure[6-b]** **Figure[6-c]**
X = 5 **X = 10** **X = 15**

Figure[6] Thermoelectric power vs. Temperature of the hot End for $Ge_{20}Bi_xSe_{80-x}$ Thin Films

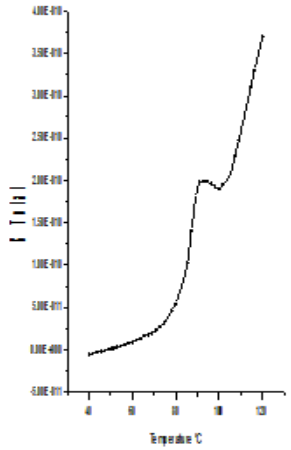

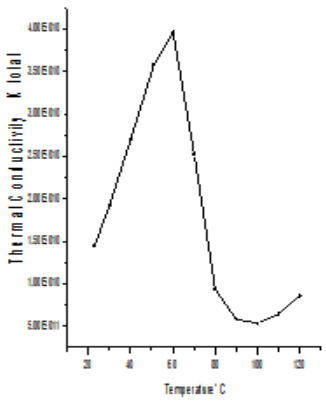

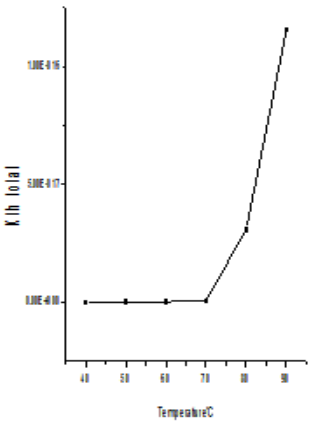

Figure[7-a] **Figure[7-b]** **Figure[7-c]**
X = 5 **X = 10** **X = 15**

Figure 7 : Thermal Conductivity vs. Temperature for Ge20BixSe80-x Thin Films

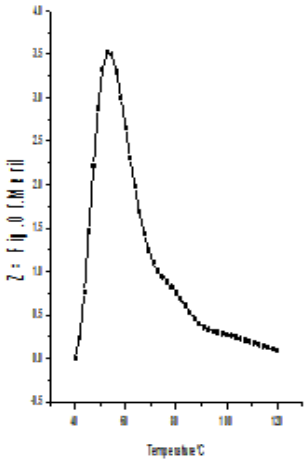

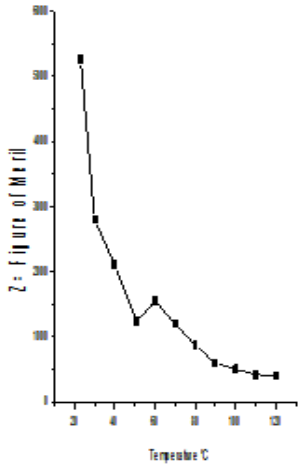

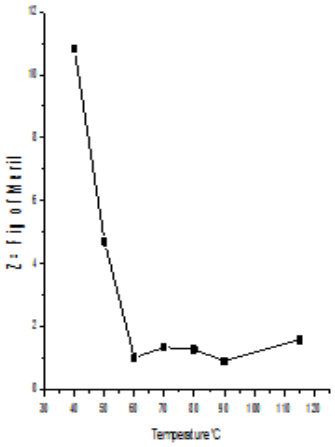

Figure[8-a] **Figure[8-b]** **Figure[8-c]**
X = 5 **X = 10** **X = 15**

Figure[8]:Figure of Merit vs. Temperature for Ge20BixSe80-x Thin Films

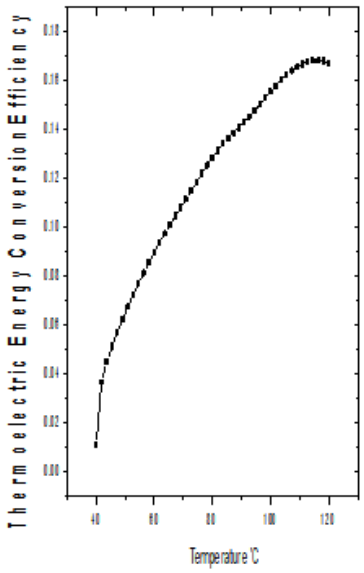

Figure[9-a]
X = 5

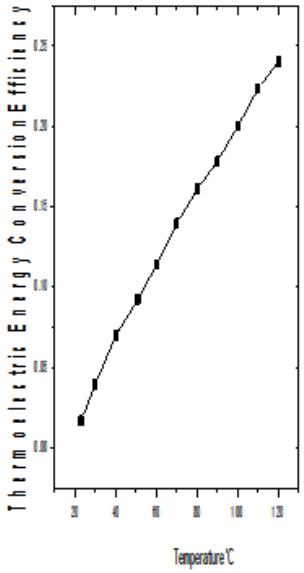

Figure[9-b]
X = 10

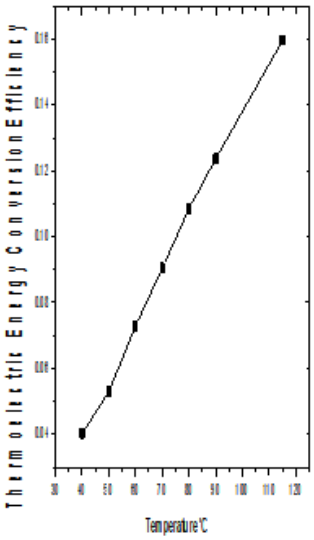

Figure[9-c]
X = 15

Figure[9]: ThermoElectric Energy Conversion Optimum Efficiency vs. Temperature for Ge20BixSe80-x Thin Films

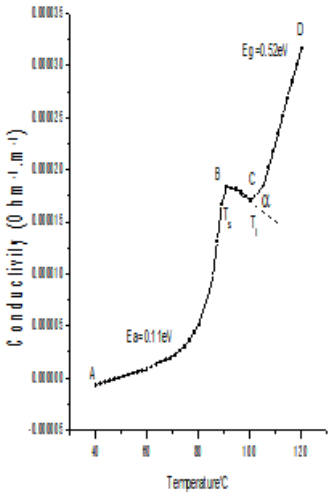

Figure[10-a]
X = 5

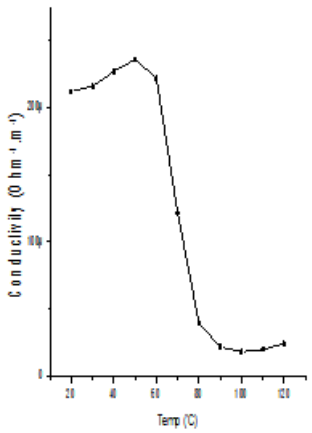

Figure[10-b]
X = 10

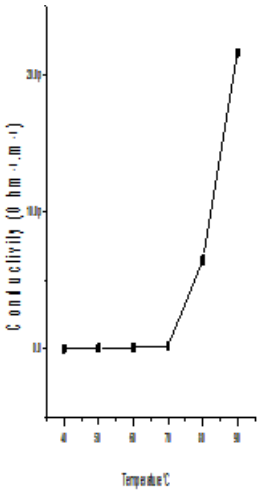

Figure[10-c]
X = 15

Figure 10 : Electrical Conductivity vs Temperature for Ge20BixSe80-x Thin Films

Table 1:

Film Thickness Bi=5%	**E_g (eV)**	**E_o (eV)**	**E_d (eV)**	**n_o**	**ε_∞**
260 nm	1.73	3.34	24.04	2.86	8.19
273 nm	1.56	3.12	24.14	2.96	8.74
393 nm	1.52	3.04	23.96	2.98	8.88
576 nm	1.34	2.68	23.00	3.09	9.58

Table 2:

Film Thickness Bi=10%	**E_g (eV)**	**E_o (eV)**	**E_d (eV)**	**n_o**	**ε_∞**
255 nm	0.87	1.74	19.82	3.52	12.38
284 nm	0.84	1.68	19.61	3.56	12.67
328 nm	0.87	1.74	22.41	3.72	13.88

Table 3:

Film Thickness Bi=15%	**E_g (eV)**	**E_o (eV)**	**E_d (eV)**	**n_o**	**ε_∞**
232 nm	0.564	1.128	1.902	1.639	2.686
280 nm	0.355	0.710	3.413	2.407	5.793
385 nm	1.099	2.198	12.279	2.566	6.584

Table[4]:

Bi %	**$E=E_a-E_f$ Jouls**	**E_μ Jouls**
5	1.566E-20	3.76E-20
10	11E-19	2.5E-18
15	1.465E-18	1.157E-18